PNAS RESEARCH ARTICLE | IMMUNOLOGY AND INFLAMMATION

# Redox status regulates autophagy in thymic stromal cells and promotes T cell tolerance

Manpreet K. Semwal[a,b,1,2], Allison K. Hester[a,c,1], Yangming Xiao[a], Chioma Udeaja[a], Sergio Cepeda[d], John S. Verschelde II[a], Nicholas Jones[a], Sarah A. Wedemeyer[a], Simon Emtage[a], Kymberly Wimberly[a], and Ann V. Griffith[a,2,3]

Edited by Yousuke Takahama, National Cancer Institute, NIH, Bethesda, Maryland; received March 11, 2022; accepted August 30, 2022 by Editorial Board Member Philippa Marrack

**Thymic stromal cells (TSCs) are critical regulators of T cell tolerance, but their basic biology has remained under-characterized because they are relatively rare and difficult to isolate. Recent work has revealed that constitutive autophagy in TSCs is required for self-antigen presentation and central T cell tolerance induction; however, the mechanisms regulating constitutive autophagy in TSCs are not well understood. Hydrogen peroxide has been shown to increase autophagy flux in other tissues, and we previously identified conspicuously low expression of the hydrogen peroxide–quenching enzyme catalase in TSCs. We investigated whether the redox status of TSCs established by low catalase expression regulates their basal autophagy levels and their capacity to impose central T cell tolerance. Transgenic overexpression of catalase diminished autophagy in TSCs and impaired thymocyte clonal deletion, concomitant with increased frequencies of spontaneous lymphocytic infiltrates in lung and liver and of serum antinuclear antigen reactivity. Effects on clonal deletion and autoimmune indicators were diminished in catalase transgenic mice when autophagy was rescued by expression of the Becn1$^{F121A/F121A}$ knock-in allele. These results suggest a metabolic mechanism by which the redox status of TSCs may regulate central T cell tolerance.**

thymus | tolerance

## Significance

Thymic stromal cells impose T cell self-tolerance by presenting self-antigens to developing T cells and inducing apoptosis in strongly self-reactive cells, a process known as clonal deletion. Self-antigen presentation is facilitated by particularly high levels of basal autophagy in thymic stromal cells, but the mechanisms regulating this constitutive autophagy have not been clear. Here, we find that high basal autophagy in thymic stromal cells depends on conspicuously low expression of the hydrogen peroxide–quenching enzyme catalase and that the highly oxidative redox status of thymic stromal cells promotes T cell clonal deletion and self-tolerance in an autophagy-dependent manner. These studies suggest that tightly regulated catalase expression promotes thymic stromal cell autophagy and central T cell tolerance.

Despite the critical roles played by thymic stromal cells (TSCs) in steady-state T cell differentiation, their biology is still relatively under-characterized. This is due, in part, to the fact that stromal cells are very rare, representing less than 1% of total thymic cellularity. Isolation of stromal cells requires extensive enzymatic treatments (1) that have been shown to induce important changes in their biology. Indeed, even simple removal of stromal cells from their native three-dimensional architecture induces profound changes (2). To overcome these barriers, we previously developed a computational deconvolution approach to estimate the global stromal gene expression signature in the thymus (3). We found that TSCs, especially those in the cortex, express conspicuously low levels of the hydrogen peroxide ($H_2O_2$)–quenching enzyme catalase, acquire high levels of oxidative damage (including high levels of 8-hydroxy-2-deoxyguaniosine), and have greater sensitivity to reactive oxygen species (ROS)–induced mitochondrial damage relative to lymphocytes from the same thymus (4). Several lines of evidence suggest an unusual redox environment in TSCs (reviewed in refs. 5 and 6). TSCs, particularly in the cortex, are continuously exposed to developing T cells that are undergoing high rates of cell division (7, 8). As a result, stromal cells, unlike lymphoid cells, which quickly exit the cell cycle and emigrate (9), persist in a state of exposure to the cell-permeable products of metabolism and cell division, including $H_2O_2$ (10), and may therefore experience particularly high ROS levels. A similar scenario has been demonstrated in the bone marrow (BM), where Cx43-dependent channels facilitate transfer of ROS from proliferating hematopoietic stem cells to adjacent BM stromal cells, a function critical for hematopoietic regeneration (11). The unusually highly oxidative environment present in the thymus (4, 12) suggests that there may be a physiological function for low catalase expression in TSCs.

Among ROS, $H_2O_2$ has a relatively long half-life and is cell permeable, making it an important secondary messenger in maintaining cellular homeostasis (13). Several studies have shown that moderate levels of ROS play crucial physiological roles in many different biological processes, both at the transcriptional and translational levels (13, 14), and can promote autophagy specifically in several ways. Upon nutrient starvation, $H_2O_2$ not only acts as an early inducer of autophagy but also as the main transducer of intracellular signals promoting autophagy (15–18). In the presence of $H_2O_2$, inactive AMP-activated protein kinase (AMPK) is converted to active AMPK, leading to the formation of the Unc-51–like autophagy-activating kinase 1 (ULK1) complex,

Author contributions: M.K.S. and A.V.G. designed research; M.K.S., A.K.H., Y.X., C.U., S.C., J.S.V., N.J., S.A.W., S.E., K.W., and A.V.G. performed research; M.K.S., A.K.H., Y.X., S.C., S.A.W., K.W., and A.V.G. analyzed data; and M.K.S., A.K.H., Y.X., S.C., S.A.W., and A.V.G. wrote the paper.

The authors declare no competing interest.

This article is a PNAS Direct Submission. Y.T. is a Guest Editor invited by the Editorial Board.



See online for related content such as Commentaries.

[1]M.K.S. and A.K.H. contributed equally to this work.

[2]M.K.S. and A.V.G. are co-corresponding authors.

[3]To whom correspondence may be addressed. Email: griffitha3@uthscsa.edu.

This article contains supporting information online at http://www.pnas.org/lookup/suppl/doi:10.1073/pnas.2204296119/-/DCSupplemental.

Published September 26, 2022.

which is required for autophagosome formation (16). $H_2O_2$ also initiates oxidation of autophagy-related (Atg) 4, which leads to the inactivation of its delipidating activity on LC3, further promoting the structural integrity of the mature autophagosome (17, 19). $H_2O_2$ can also initiate autophagy by altering the thiol redox state (16, 20), by inhibiting phosphoinositide 3-kinases/protein kinase B/mechanistic target of rapamycin (PI3K/Akt/mTOR) signaling (21), and by inducing beclin-1 expression, which leads to the formation of a complex between beclin-1 and a class III PI3K, an important step for initiating autophagy (22).

Recent work has established that TSCs exhibit an unusually high level of basal autophagy in the steady state (23, 24) and that constitutive autophagy in TSCs is required for self-antigen presentation and central T cell tolerance induction (24, 25). However, the mechanisms regulating constitutive autophagy in TSCs are not well understood. Together, these observations led to the hypothesis that the high levels of $H_2O_2$ in TSCs established by low catalase expression may represent the mechanism promoting the conspicuously high levels of basal autophagy required for self-antigen presentation and T cell tolerance induction.

## Results

**Catalase Regulates Mitochondrial $H_2O_2$-Quenching Capacity in TSCs.** Our previous work revealed that TSCs, especially those in the cortex, express conspicuously low levels of the $H_2O_2$-quenching enzyme catalase, acquire high levels of oxidative damage, and have greater sensitivity to ROS relative to lymphocytes from the same thymus (4). Since we hypothesized that low catalase expression promoted the high $H_2O_2$ levels in TSC populations, we tested whether mice overexpressing a mitochondrially targeted human catalase transgene (mCat Tg) (26) had an increased capacity to quench exogenous $H_2O_2$. We used the fluorescent chemical probe mitochondria peroxy yellow 1 (MitoPY1) to establish the capacity of distinct populations of cells within the thymus to quench mitochondrial $H_2O_2$, by directly measuring mitochondrial $H_2O_2$ after gentle treatment with $H_2O_2$ (150 mM for 30 min). Thymic lymphocytes, medullary epithelial cells (mTECs), cortical epithelial cells (cTECs), and dendritic cells (DCs) were analyzed by flow cytometry (Fig. 1*A*). Though mean catalase activity was previously only found to increase by ∼25% in heart mitochondria from mCat Tg mice (26), we saw a significant reduction in mitochondrial $H_2O_2$ in cTECs and DCs from mCat Tg mice relative to the wild type (WT), whereas decreases in lymphocytes and mTECs were not statistically significant (Fig. 1 *B*–*E*). Together, these results suggest that changes in catalase expression are sufficient to modulate $H_2O_2$ levels in TSC, including thymic DCs and cTECs.

**Autophagy Is Regulated by Redox Status in Thymic DCs and cTECs and Is Rescued by Expression of Becn1$^{KI}$ Alleles in mCat Tg Mice.** Since high $H_2O_2$ can promote autophagy induction (18), we next sought to test whether autophagy levels in various thymic populations correlated with mitochondrial $H_2O_2$ levels. We used an autophagy reporter mouse model (GFP-LC3 Tg mice) in which transgenic expression of a GFP-LC3 fusion protein allows fluorescent labeling of autophagosomes (23). In flow cytometry experiments, decreased GFP fluorescence is often associated with degradation of autophagosomes and increased autophagy flux after treatment (27). However, we reasoned that in our studies, in which freshly isolated cells were examined in the absence of exogenous treatments to promote or inhibit autophagy, differences in GFP fluorescence could represent either differences in autophagosome generation, which would increase fluorescence, or differences in autophagosome fusion with lysosomes and degradation, which would decrease fluorescence. Since stimulation of T cells is known to induce autophagy (28), we first evaluated whether we could measure increased autophagosome formation using a cytometric approach in GFP-LC3 Tg mice. Using splenic T cells isolated from WT and GFP-LC3 Tg mice after in vitro stimulation with anti-CD3 and anti-CD28 antibodies for 24 h, we confirmed that changes in autophagy could be measured by comparing GFP fluorescence in unstimulated and stimulated cells using both flow cytometry and microscopy. Stimulated cells developed GFP$^+$ populations among CD69$^+$ cells and had increased GFP median fluorescence intensity (MFI) when assessed by flow cytometry at 24 h after stimulation, which subsequently decreased after 48 h (*SI Appendix*, Fig. S1 *A* and *B*). Autophagic punctae were also increased 24 h after stimulation relative to unstimulated cells by microscopy (*SI Appendix*, Fig. S1 *C* and *D*). Quantification of autophagy in stimulated cells was similar when evaluated by comparing either the frequency of punctae-positive cells by microscopy (*SI Appendix*, Fig. S1*D*), the frequency of GFP$^+$ cells established by flow cytometry (*SI Appendix*, Fig. S1*E*), or the GFP MFI by flow cytometry (*SI Appendix*, Fig. S1*F*). To test this approach in distinct populations of freshly isolated thymic cells, we evaluated GFP expression in thymic lymphocytes and thymic epithelial cells (TECs) from WT and GFP-LC3 Tg mice. Since TECs exhibit higher GFP autofluorescence relative to lymphocytes (*SI Appendix*, Fig. S2*A*, *Left*, and S2*B*, gray histograms), we normalized GFP MFI in each GFP-LC3 Tg sample to a WT sample of the same cell type (lymphocyte or TEC) from the same experiment (*SI Appendix*, Fig. S2*C*). We found that autophagy levels were ∼10-fold higher in TECs relative to lymphocytes (*SI Appendix*, Fig. S2*C*). These results are consistent with those of earlier studies that showed a high frequency of autophagy-positive cells in TECs and very little to no autophagy in thymic lymphocytes in the steady-state thymus (23, 24). These results support the use of this flow cytometric approach to evaluate autophagy in distinct thymic cellular populations.

To test whether catalase expression regulates the levels of autophagy in the thymus, we compared GFP expression in lymphocytes, DCs, cTECs, and mTECs in mCat Tg and mCat non-Tg mice bearing the GFP-LC3 transgene. For cTECs, mTECs, and lymphocytes, GFP MFI in each sample was normalized to the same cellular subset in GFP-LC3 nonreporter mice in the same experiments. For DCs, where GFP-LC3 nonreporter mice were not analyzed together with the other groups, GFP MFI was normalized to the MFI in total TEC from mCat non-Tg samples from the experiment (see histograms in Fig. 2*A*). We found decreased autophagy in cTECs and DCs of mCat Tg mice when compared with non-Tg mice (Fig. 2 *C* and *D*, respectively), but no differences were found between mCat Tg and non-Tg lymphocytes and mTECs (Fig. 2 *B* and *E*, respectively). These results suggest that catalase expression regulates autophagy in cTECs and thymic DCs but not in lymphocytes or mTEC.

Testing whether potential downstream effects of catalase expression on T cell development were dependent on changes in autophagy required a means of independently manipulating autophagy levels in catalase transgenic mice. To accomplish this, we employed a recently developed transgenic mouse model in which a Phe121Ala mutation was introduced to the beclin 1

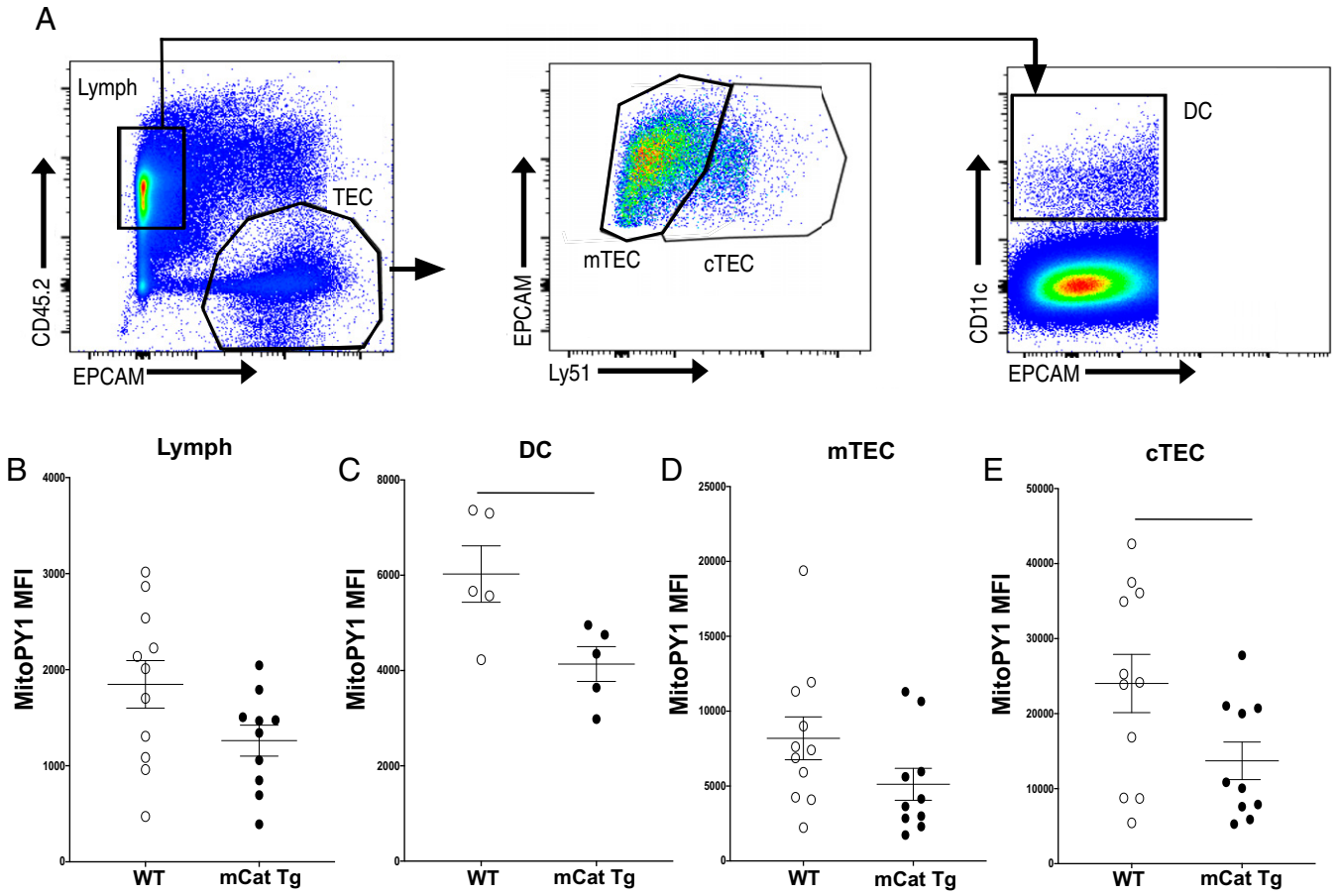


**Fig. 1.** Mitochondrial $H_2O_2$–quenching capacity is significantly diminished by catalase overexpression in DCs and cTECs. (*A*) Representative surface CD45.2, EPCAM, Ly51, and CD11c staining in single-cell suspensions from mouse thymus after enzymatic digestion and mechanical lymphocyte depletion (gated on viable singlets) treated with 150 μm of $H_2O_2$. (*B–E*) Measure of mitochondrial $H_2O_2$ indicated by MitoPY1 MFI in thymic populations treated with 150 μm of $H_2O_2$ in (*B*) lymphocytes in WT ($n = 11$) and mCat Tg ($n = 10$) mice, (*C*) DCs in WT ($n = 5$) and mCat Tg ($n = 5$) mice, (*D*) mTEC in WT ($n = 11$) and mCat Tg ($n = 10$) mice, and (*E*) cTEC in WT ($n = 11$) and mCat Tg ($n = 10$) mice. (*B–E*) Horizontal bar indicates Student's two-tailed *t* test, $P < 0.05$. $P = 0.026$ and 0.042 for DCs and cTECs, respectively. Mean and SEM are indicated by horizontal lines. Data are representative of three or more experiments. Each symbol represents an individual mouse.

gene ($Becn1^{F121A/F121A}$) (29). This mutation inhibits the interaction of Becn1 with its negative regulator BCL2, resulting in increased basal autophagy. $Becn1^{F121A/F121A}$ KI (herein referred to as $Becn1^{KI/KI}$) mice were crossed with GFP-LC3 reporter mice to allow autophagy measurement. To test whether the reduced autophagy in mCat Tg mice could be rescued by introducing the $Becn1^{KI}$ allele, we crossed mCat Tg mice with $Becn1^{KI/KI}$ GFP-LC3 Tg mice to generate mCat Tg mice expressing both $Becn1^{KI}$ and GFP-LC3 alleles (mCat Tg:$Becn1^{KI/KI}$:GFP-LC3). We found that the decreased autophagy we observed in mCat Tg stromal cells was significantly rescued by expression of two $Becn1^{KI}$ alleles in DCs (Fig. 2*C*). The decreased autophagy we observed in mCat Tg cTECs was partially rescued by expression of two $Becn1^{KI}$ alleles in cTECs, and there were no significant differences between $Becn1^{KI/KI}$ and either mCat Tg or mCat non-Tg groups (Fig. 2*D*).

We interpreted increased GFP fluorescence in our system as reflecting increased autophagosome formation rather than decreased autophagy flux for several reasons. First, our results in *SI Appendix*, Figs. S1 and S2 are consistent with other work that has demonstrated higher levels of basal autophagy in stromal cells relative to lymphocytes, as well as the induction of autophagy upon T cell stimulation. Second, decreased GFP fluorescence corresponded to cells in with lower levels of $H_2O_2$ (in mCat Tg mice relative to WT), and $H_2O_2$ is a known inducer of autophagy initiation (17). Finally, the Becn1KI allele has been shown to increase autophagy in other tissues (29) and corresponds with higher GFP fluorescence in our system. Together, these studies indicate that autophagy levels can be regulated by catalase expression and that the decreased autophagy in mCat Tg mice is rescued by expression of the $Becn1^{KI}$ allele.

To compare our flow cytometric approach to a microscopy-based approach for evaluating autophagy, we compared autophagic punctae in GFP-LC3 Tg mice on the mCat Tg and mCat non-Tg background. Since cTECs have much higher levels of autophagy than do lymphocytes, which exhibit almost no basal autophagy (24), we reasoned that cortical autophagy measured by microscopic identification of $GFP^+$ punctae would almost exclusively represent stromal, rather than lymphocyte, autophagy. To compare $GFP^+$ punctae in the cortex of GFP-$LC3^+$ mCat Tg and non-Tg mice, we employed a recently described differences of Gaussian blurs technique to better distinguish $GFP^+$ punctae in cells (30). Image J software was used to measure total cortical area and to count the number of punctae, as shown in Fig. 3*A*. We found that mCat Tg thymi had a lower frequency of $GFP^+$ punctae per cortical area relative to mCat non-Tg mice (Fig. 3*B*), consistent with decreased autophagy in mCat Tg animals. In addition, to distinguish between diminished autophagosome formation and increased

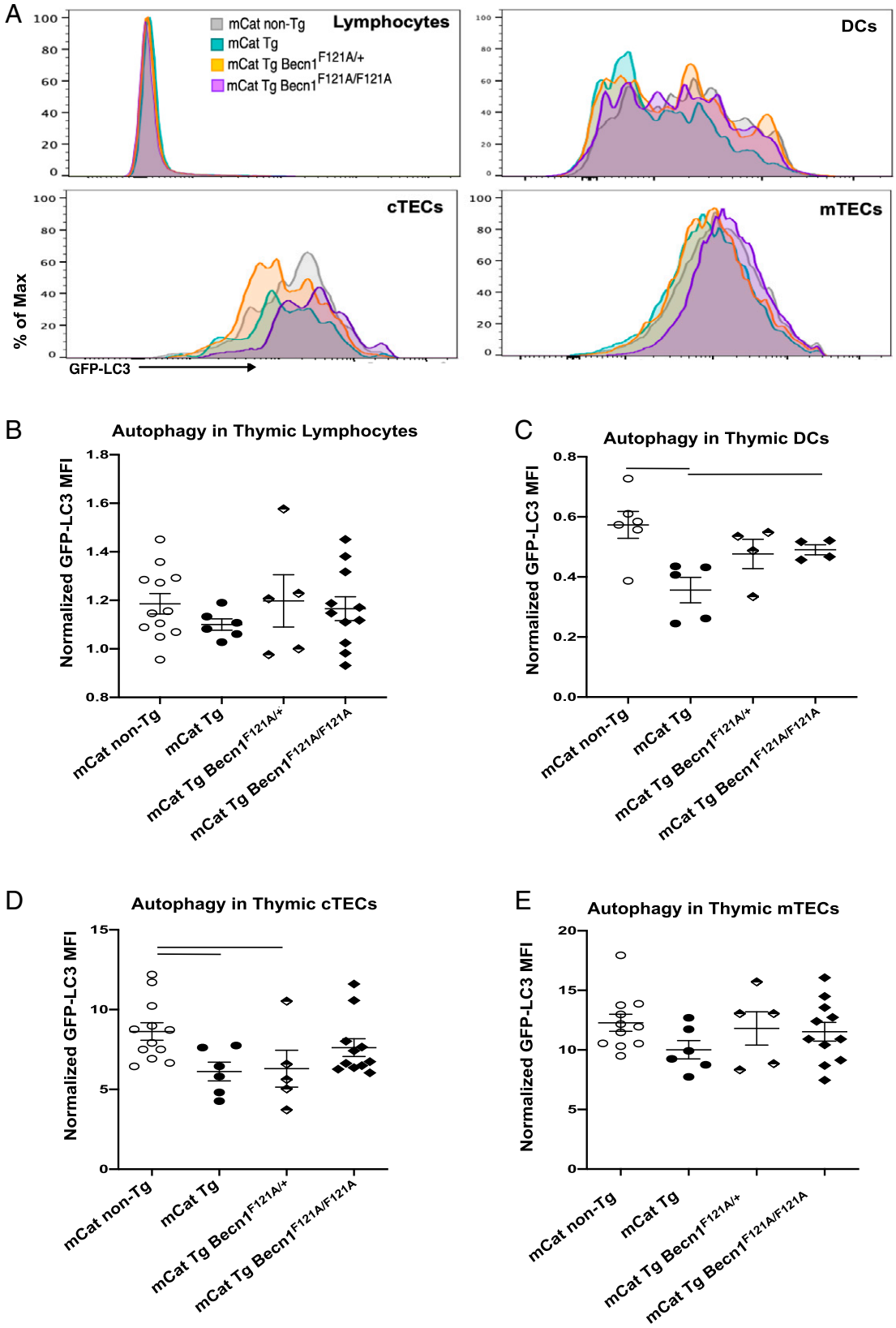


**Fig. 2.** Autophagy is regulated by redox status in thymic DCs and cTECs and is partially rescued by expression of Becn1$^{F121A}$ KI alleles in mCat Tg mice. (*A*) Representative histograms of GFP fluorescence from the indicated cell types of GFP-LC3$^{+}$ mice of the indicated genotypes: mCat non-Tg (gray), mCat Tg (turquoise), mCat Tg Becn1$^{F121A/+}$ (orange), and Becn1$^{F121A/F121A}$ (purple). (*B–E*) Autophagy indicated by GFP-LC3 MFI in (*B*) lymphocytes, (*C*) DCs, (*D*) cTECs, and (*E*) mTECs of GFP-LC3 (mCat non-Tg, open circles; $n$ = 5–12), GFP-LC3 reporter mice expressing the mCat Tg alone (mCat Tg, filled circles; n = 4–6), mCat Tg and one Becn1$^{F121A}$ KI allele (mCat Tg Becn1$^{F121A/+}$, half-filled diamond; $n$ = 4–5), and in mCat Tg Becn1$^{F121A}$ homozygotes (mCat Tg Becn1$^{F121A/F121A}$, filled diamond; $n$ = 4–11). The MFI in each sample in *B*, *D,* and *E* was normalized to MFI in GFP-LC3 nonreporter mice (WT B6 control) samples from the same experiment. (*C*) MFI in each sample was normalized to TEC samples from mCat non-Tg samples from the same experiment. Mean and SEM are indicated by horizontal lines. Horizontal bars indicate one-way ANOVA Fisher's LSD, $P < 0.05$. (*B–E*). Data are representative of three or more experiments. Each symbol represents an individual mouse. Max, maximum.

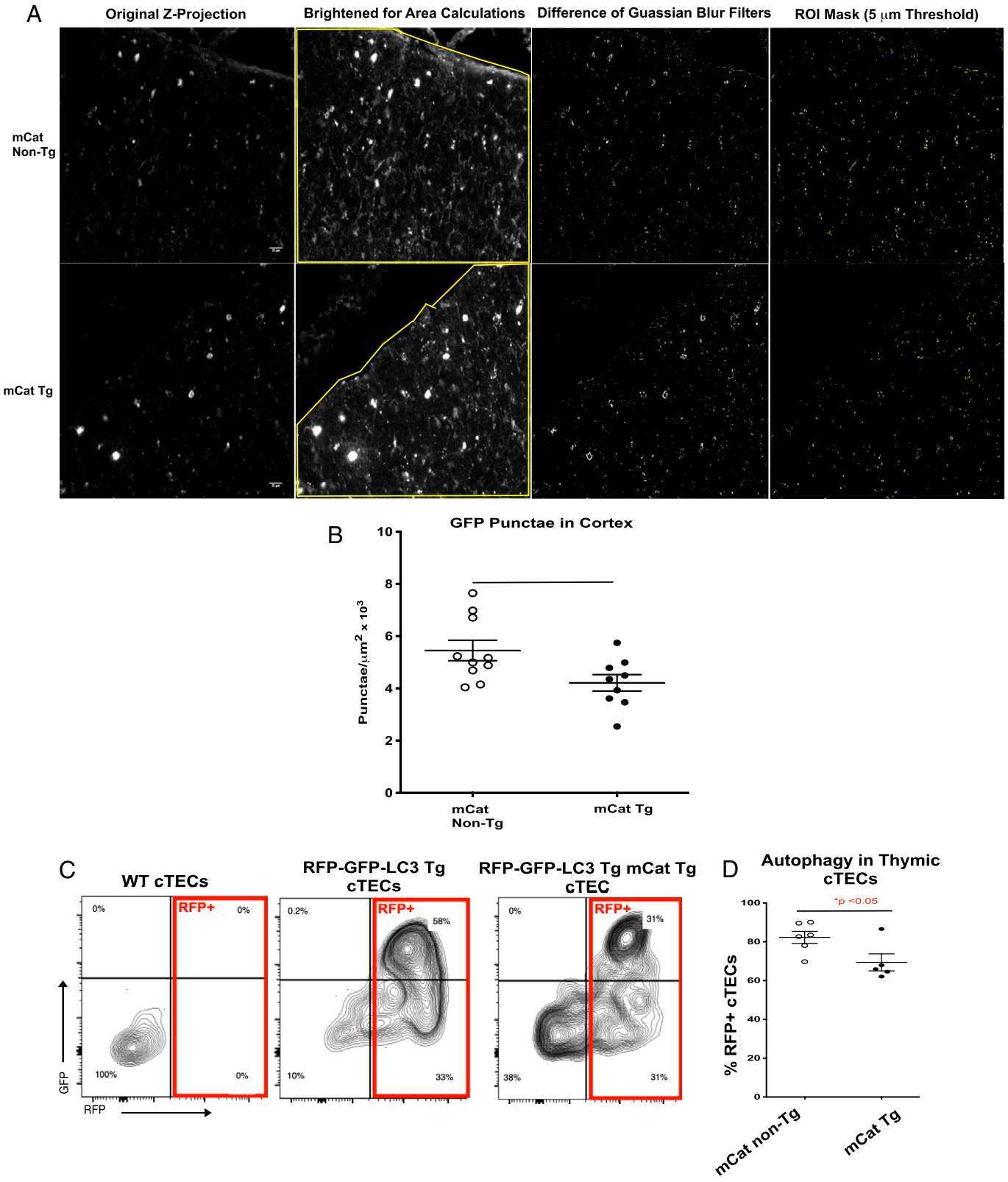


**Fig. 3.** Reduced autophagy in mCat Tg thymus. Autophagy was assessed by quantifying GFP$^+$ punctae in GFP-LC3$^+$ mCat non-Tg and mCat Tg thymi. (*A*) Representative images of original Z-stack images from mCat non-Tg (*Top*) and mCat Tg (*Bottom*) GFP-LC3$^+$ reporter mice , representative images with brightness increased to measure thymic tissue area (yellow lines), representative images after applying differences of two Gaussian blur filters to better distinguish punctae (as described in *Materials and Methods*), and representative image of particle analysis ROIs identified in Image J. (*B*) Aggregated data from GFP punctae in cortex. (*C*) Representative RFP fluorescence in WT, RFP-GFP-LC3 mCat non-Tg, and RFP-GFP-LC3 mCat Tg cTECs (gated as in Fig. 1). (*D*) Frequency of total RFP$^+$ cTECs. Mean and SEM are indicated by horizontal lines. Horizontal lines indicate significant differences ($P < 0.05$) by Student's *t* test.

autophagosome degradation, we crossed mCat Tg mice to a second autophagy reporter strain bearing the red fluorescence protein (RFP)–GFP-LC3 fusion gene (31) to evaluate both autophagosomes and autolysosomes. Since GFP fluorescence is quenched in the autolysosome while RFP fluorescence persists, autophagosomes (GFP$^+$RFP$^+$) and autolysosomes (GFP-RFP$^+$)

may be distinguished in this model. When we compared GFP and RFP expression in cTECs from mCat Tg and non-Tg mice, we found that the decrease in GFP fluorescence in mCat Tg mice reflected a marked increase in GFP- RFP- double-negative cells not undergoing autophagy rather than an accumulation of GFP-RFP$^{+}$ cells with high frequencies of autolysosome activity (Fig. 3 *C* and *D*).

**Normal Positive Selection in mCat Tg Mice at the Population Level.** Since autophagy promotes positive selection of thymocytes (24), we evaluated whether the decrease in autophagy in mCat Tg TSCs was sufficient to impair positive selection in this model. To quantify positive selection at the population levels, we measured the frequency of postpositive selection thymocytes among the DP (CD4+ CD8+ double positive) population using CD3 and CD69 as indicators of the postpositive selection subset (32, 33). As shown in *SI Appendix*, Fig. S3, the frequency of postpositive selection DP thymocytes was normal in mCat Tg thymi, indicating the decrease in autophagy in mCat Tg mice was not sufficient to impart major impairments in positive selection. This approach may not detect subtle changes in positive selection however, and detection of such subtle changes may require further examination in transgenic T cell receptor models, as has been shown for mouse models in which TSCs are fully deficient in their ability to perform autophagy (24).

**Redox Status Regulates Early and Late Clonal Deletion in an Autophagy-Dependent Manner.** To address whether the diminished autophagy we found in mCat Tg TSCs was physiologically relevant for negative selection of potentially autoreactive T cells, we employed a recently reported flow cytometric approach to measure thymocyte clonal deletion. To measure clonal deletion in the polyclonal T cell population, this approach identifies cleaved caspase 3 among signaled (TCRβ$^{hi}$CD5$^{hi}$) thymic T cells (after exclusion of cells expressing CD25, NK1.1, and TCRγδ; see ref. 34) (Fig. 4*A*). Such flow cytometric approaches allow the evaluation of selection at the population level in a natural polyclonal repertoire (34, 35). We further divided signaled cells into early (CCR7$^{-}$) or late (CCR7$^{+}$) stages (36–39). We found that the frequency of both early and late clonally deleted cells declined in mCat Tg mice relative to non-Tg mice and was rescued in mCat Tg:Becn1$^{KI/KI}$ mice, although the magnitude of the decrease and rescue among early (CCR7$^{-}$) signaled thymocytes was greater than that in late (CCR7$^{+}$) signaled thymocytes (Fig. 4 *B* and *C*). This suggests a catalase-mediated decline in clonal deletion that has a greater impact during the early stages of negative selection than during later stages. Since differences in autophagy were found in stromal but not lymphocyte populations, these results support the notion that the redox status of TSCs promotes high basal autophagy within these populations that, in turn, promotes clonal deletion in developing T lymphocytes.

Autophagy is critical for antigen presentation, especially during MHC class II presentation to CD4$^{+}$ T cells (25, 40); therefore, diminished autophagy could be predicted to cause a particular decrease in the efficiency of negative selection of CD4 T cells. We measured the frequency of single positive (SP) CD4 and CD8 T cells in mCat Tg mice and found an increase in the frequency of SP CD4$^{+}$ T cells in mCat Tg thymi relative to those from non-Tg mice. This increase was rescued in mice bearing the Becn1$^{KI}$ allele (Fig. 4 *D* and *E*), indicating a potential autophagy-mediated increase in deletion of potentially autoreactive CD4$^{+}$ T cells in mCat Tg mice bearing the Becn1$^{KI}$ allele. Since changes in selection of CD4 T cells could affect the development of FoxP3$^{+}$ regulatory T (Treg) cells (41, 42), we evaluated the frequency of FoxP3$^{+}$ Tregs among SP CD4 T cells in the thymus, peripheral blood, and secondary lymphoid organs in mCat Tg and non-Tg mice but found no significant differences (*SI Appendix*, Fig. S4). The frequency of SP CD8 T cells trended downward in mCat Tg mice relative to non-Tg mice, but this difference was not statistically significant (Fig. 4*E*). The frequency of SP CD8 T cells was significantly decreased in mCat Tg:Becn$^{KI/+}$ but not mCat Tg:Becn1$^{KI/KI}$ mice, although the biological significance of this difference is currently unclear.

Thymic DCs are heterogenous at steady state, and distinct subsets have unique roles in T cell tolerance induction (43–49). Further, the relative abundance of DC subsets varies over the course of development and in responses to stressors (50, 51). Given the impaired clonal deletion we observed in mCat Tg mice, we therefore evaluated the overall frequency of DC subsets in Cat Tg and non-Tg mice. Using B220 and CD11c to distinguish plasmacytoid and conventional DCs (cDCs; see ref. 52), we did not find differences in the overall frequencies of these population in Cat Tg mice (*SI Appendix*, Fig. S5 *A–C*). Among cDCs, we evaluated the frequency of Sirpα$^{+}$ and Sirpα$^{-}$ subsets (53), which also appeared normal in Cat Tg mice (*SI Appendix*, Fig. S5 *D* and *E*). Since late negative selection could be affected by impaired migration of thymocytes and DCs into medullary areas in Cat Tg mice, we also evaluated the expression of *Ccl19* and *Ccl21a*, which promote medullary migration of CCR7-expressing cells (39, 54–56), in sorted mTECs from Cat Tg and non-Tg mice. We found that *Ccl21a* expression was not significantly changed in Cat Tg mTEC, and *Ccl19* was somewhat increased in Cat Tg relative to non-Tg mTECs (*SI Appendix*, Fig. S5 *G* and *F*, respectively). It therefore seems unlikely that impaired medullary migration or altered DC subset abundance mediate the decreased clonal deletion found in the mCat Tg mice.

**Distinct Redox Regulation of Early and Late Clonal Deletion.** Our clonal deletion experiments suggest that negative selection is impaired in mCat Tg mice. Since catalase is overexpressed in both stromal and lymphoid cells in the thymus of mCat Tg mice, we performed reciprocal bone marrow transplant (BMT) experiments to test whether differences in clonal deletion were mediated by catalase overexpression in stromal cells, hematopoietic cells, or both. We transferred T cell–depleted WT or mCat Tg BM cells into irradiated WT or mCat Tg recipients. When we evaluated clonal deletion in the thymus of recipient mice 6 wk after transplant (Fig. 5*A*), we found that the frequency of early clonal deletion among CCR7$^{-}$ thymocytes declined significantly only in mice in which both the donor and recipient were mCat Tg (Fig. 5*B*), suggesting both stromal and hematopoietic cell–intrinsic roles for catalase expression in differences in early clonal deletion. Therefore, it is possible that impaired clonal deletion in mCat Tg mice requires catalase overexpression in both nonhematopoietic stromal cells, potentially cTECs or other cells we did not examine in this study, and hematopoietic stromal cells such as DCs, and possibly in lymphocyte progenitors themselves. In contrast, the frequency of late clonal deletion among CCR7$^{+}$ thymocytes was decreased even when only the recipient mouse bore the mCat transgene (Fig. 5*C*). These results suggest that redox regulation of autophagy in DCs primarily affects early rather than late clonal deletion, consistent with a potential role for DCs in mediating high levels of cortical negative selection (57) and the established role of

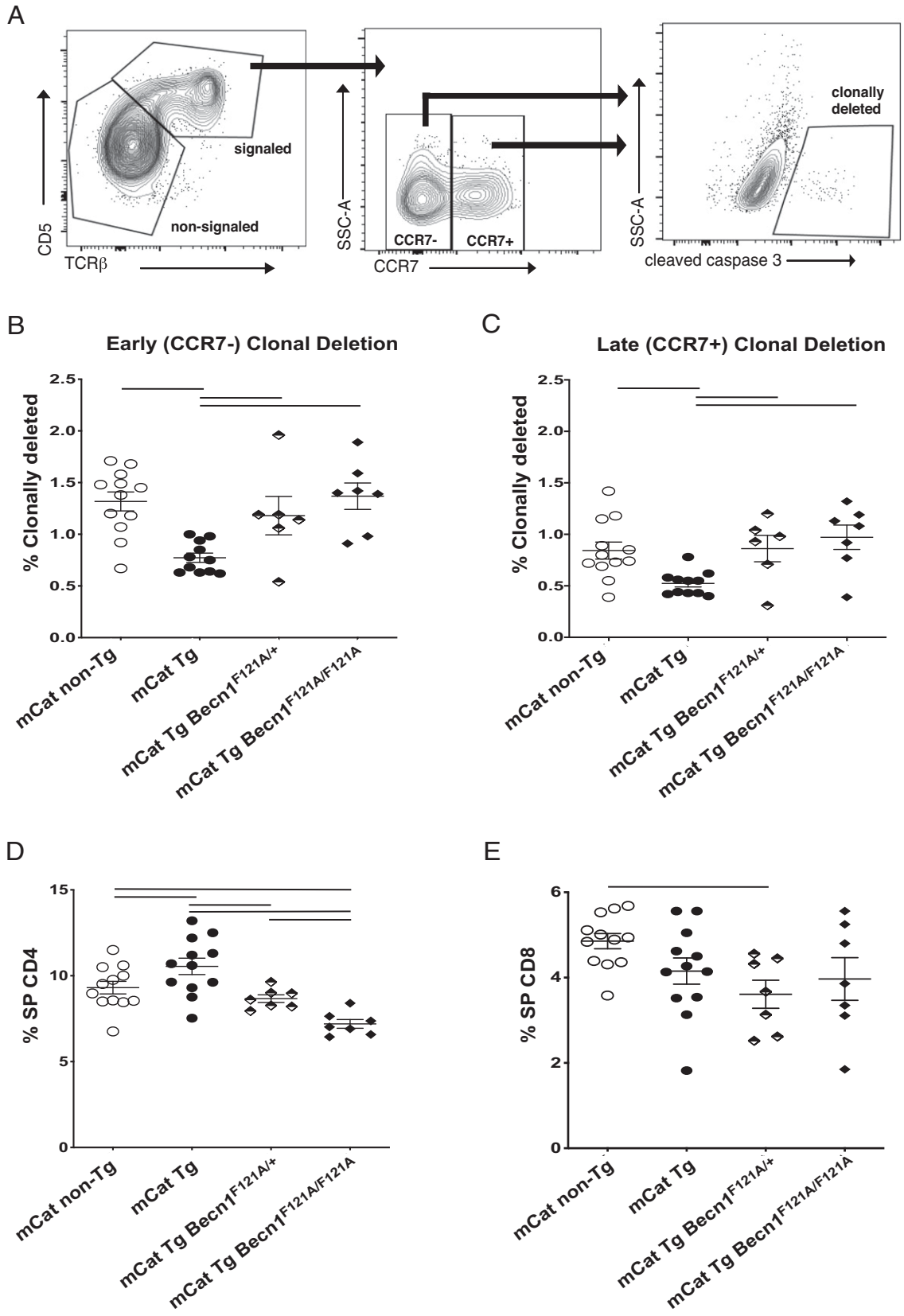


**Fig. 4.** Redox status regulates early and late clonal deletion in an autophagy-dependent manner. (*A*) The gating strategy used to identify (viable singlet, lineage negative [CD25$^-$, NK1.1$^-$, CD19$^-$, TCRg/d$^-$]) T cells undergoing early (CCR7$^-$) and late (CCR7$^+$) clonal deletion in the thymus. (*B* and *C*) Plots show frequencies of cleaved caspase-3$^+$ cells among CD5$^+$ TCRb$^+$ signaled thymocytes in (*B*) CCR7$^-$ thymocytes and (*C*) CCR7$^+$ thymocytes undergoing clonal deletion in mCat non-Tg ($n$ = 12; open circles), mCat Tg ($n$ = 12; filled circles), mCat Tg Becn1$^{F121A/+}$ ($n$ = 6; half-filled diamonds), and mCat Tg Becn1$^{F121A/F121A}$ ($n$ = 7; filled diamonds) . (*D* and *E*) The plots show frequencies of (*D*) SP CD4$^+$ thymocytes, which are increased in mCat Tg ($n$ = 12) mice relative to mCat non-Tg ($n$ = 12) mice, and are decreased in mCat Tg mice with Becn1$^{F121A/+}$ ($n$ = 6) and Becn1$^{F121A/F121A}$ ($n$ = 7); and (*E*) SP CD8$^+$ thymocytes. Mean and SEM are indicated by horizontal lines. Horizontal bars indicate one-way ANOVA Fisher's LSD, $P < 0.05$. Data are representative of three3 or more experiments. Each symbol represents an individual mouse.

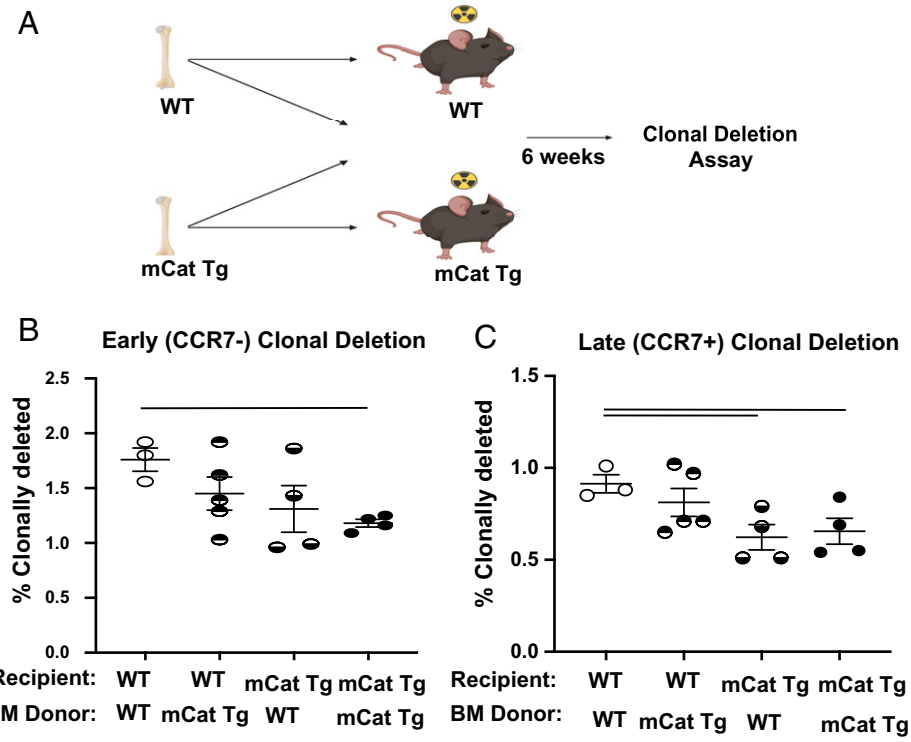


**Fig. 5.** Distinct redox regulation of early and late clonal deletion. (*A*) Schematic representation of the reciprocal BMT into the recipient mice with or without mCat Tg. T cell–depleted BM cells ($5 \times 10^6$) were transferred into the recipient mice. After 6 wk, thymus was harvested and clonal deletion was measured as mentioned in the Fig. 6 legend. Image created with Biorender. (*B* and *C*) The plots show frequency of cleaved caspase-$3^+$ among $CD5^+TCR\beta^+$ thymocytes undergoing (*B*) early and (*C*) late clonal deletion in recipient WT mice receiving BM from WT ($n = 3$; open circles) or mCat Tg ($n = 5$; top-filled circles) and in recipient mCat Tg mice receiving BM from WT ($n = 4$; bottom-filled circles) or mCat Tg ($n = 4$; filled circles) mice. Mean and SEM are indicated by horizontal lines. Horizontal bars indicate one-way ANOVA Fisher's LSD, $P < 0.05$. Data are representative of three or more experiments. Each symbol represents an individual mouse.

autophagy in MHC class II antigen presentation in DCs (58). These data also suggest that mCat overexpression in TSCs is sufficient to confer the impairment of late clonal deletion in the thymus of mCat Tg mice. The BMT results suggest this late effect is independent of the differences in autophagy we find in DCs, consistent with previous work demonstrating that DC autophagy is dispensable for negative selection of a model self-antigen (25). Although we found decreasing trends in $H_2O_2$ and autophagy in mCat Tg mTECs, the differences were not statistically significant. It may be that even the more subtle effects of catalase overexpression in mTECs were sufficient to impact late clonal deletion, but it is also possible that a different stromal cell type we did not evaluate mediates the effects on late clonal deletion.

**Increased Antinuclear Antibodies and Lymphocytic Infiltration in Aged mCat Tg Mice Are Ameliorated by Increased Autophagy.** Our hypothesis predicts that over time, mCat Tg mice would show signs of increased autoimmunity due to escape of self-reactive T cells into the periphery. To test this, we performed blinded evaluation of serum from mCat Tg mice at 6 to 8 mo of age to detect the presence of antinuclear antibodies (ANAs). We found an increase in the frequency of $ANA^+$ serum in mCat Tg mice ($n = 9$ of 14) relative to age-matched WT mice ($n = 3$ of 13), and this increase was rescued in mCat Tg:$Becn1^{KI/KI}$ mice ($n = 1$ of 7) (Fig. 6*A*).

We also performed blinded evaluation of lymphocytic infiltrates in the lungs and livers of WT, mCat Tg, and mCat Tg:$Becn1^{KI/KI}$ mice using hematoxylin and eosin (H&E) staining. We found an increase in the presence of lymphocytic infiltrates in lungs and livers of 6- to 8-mo-old mCat Tg mice relative to WT ($n = 5$ of 7 and $n = 0$ of 5 each, respectively). This increase was also partially rescued in mCat Tg:$Becn1^{KI/KI}$ mice ($n = 1$ of 7 and $n = 2$ of 7 in lung and liver, respectively) (Fig. 6 *B* and *C*). Together, these data suggest that immune tolerance is impaired in mCat Tg mice and that it is rescued by increasing basal autophagy in mCat Tg mice bearing the Becn1 KI allele (i.e., mCat Tg:$Becn1^{KI/KI}$). Together with the results of our BMT experiments, our study supports the notion that redox regulation of autophagy in TSCs is an important regulator of immune tolerance. However, since the genetic models we have used are germ-line, rather than tissue-specific, mutations, further studies will be required to reveal the relative contributions of central and peripheral mechanisms governing of these autoimmune indicators.

## Discussion

Our studies suggest that basal levels of autophagy in TSC populations are tightly regulated by catalase expression, and the studies demonstrate a role for this redox-sensitive autophagy in promoting clonal deletion and immune tolerance. Thus, promotion of constitutive autophagy in stromal cells of the steady-state thymus may represent the selective advantage conferred by the conspicuously low levels of catalase expression we previously found among these populations (4).

We show that redox regulation of autophagy is necessary for appropriate clonal deletion at both early $CCR7^-$ and later $CCR7^+$ stages of thymocyte development. Although autophagy has been suggested to play a role in antigen presentation through both MHC class I and II, its role in MHC class II antigen presentation has been more extensively studied (25,

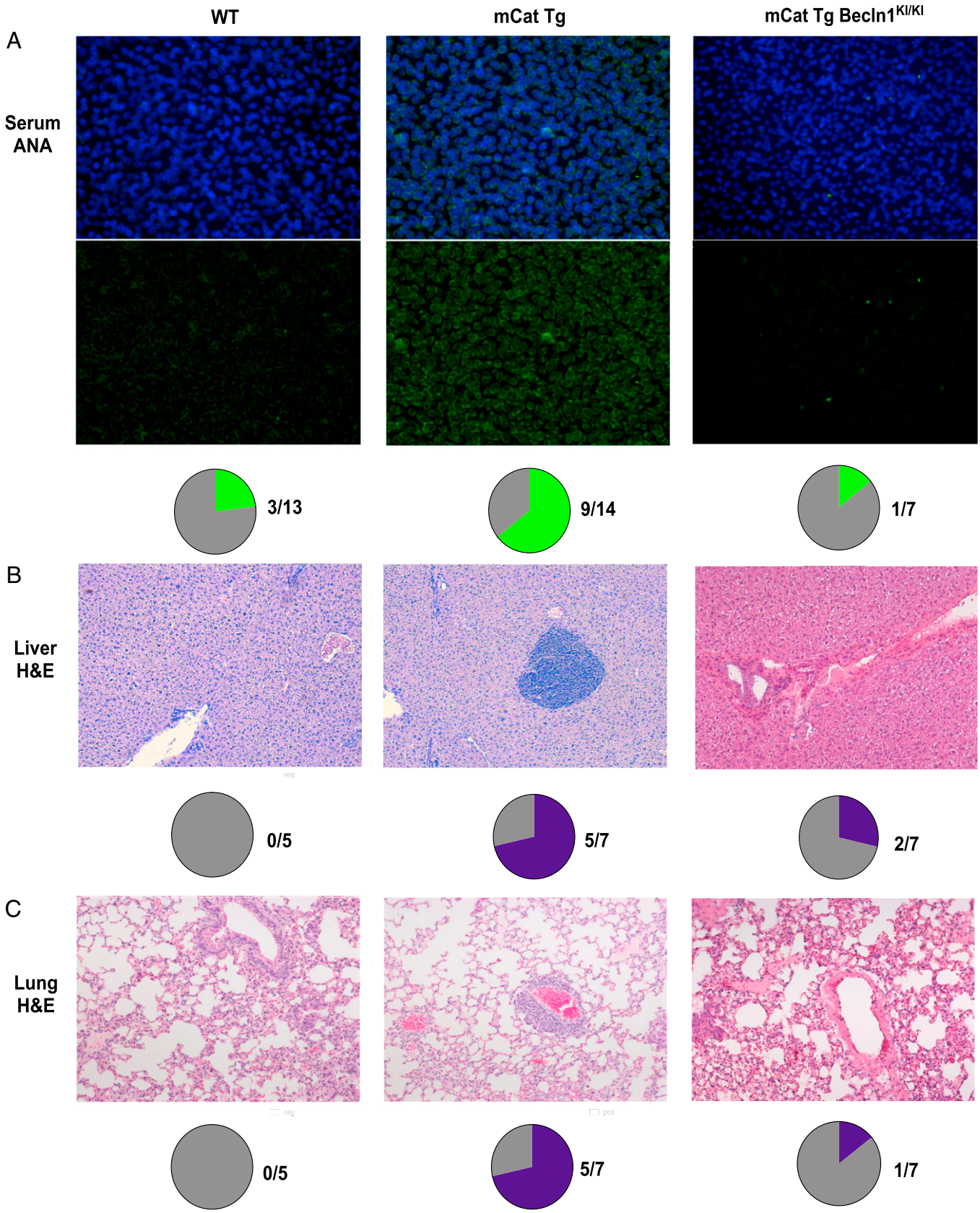


**Fig. 6.** Increased ANAs and lymphocytic infiltration in aged mCat Tg mice are ameliorated by expression of Becn1$^{F121A}$ KI alleles in mCat Tg mice. (*A*) Immunofluorescent micrographs detecting ANAs using FITC-conjugated anti-IgG in serum (1:100 dilution) from 6- to 8-mo-old WT ($n$ = 13), mCat Tg ($n$ = 14), and mCat Tg Becn1$^{KI/KI}$ ($n$ = 7) mice, using Hep-2 ANA slides. Top panels show FITC and DAPI stain together, and bottom panels show FITC staining alone. (*B* and *C*) H&E staining of (*B*) liver and (*C*) lung sections from 6- to 8-mo-old mice show increased lymphocyte infiltration in liver and lung from 6- to 8-mo-old mCat Tg mice ($n$ = 7) relative to WT ($n$ = 5), and this was rescued in mCat Tg Becn1$^{KI/KI}$ ($n$ = 7) mice. Liver and lung images were taken at ×10 magnification. In pie charts, each slice represents one mouse with negative results (gray) or with ANA (green) or lymphocytic infiltrates (purple) present.

59). Impaired clonal deletion in mCat Tg mice correlates with an expansion of SP $CD4^+$ T cells in the thymus and increased prevalence of indicators of autoreactivity, including $ANA^+$ serum and the presence of lymphocytic infiltrates in the lung and liver, consistent with previous studies showing lymphocytic infiltrates in the lungs and liver of athymic mice after transplantation of Atg5-deficient thymi (24).

Our reciprocal BMT experiment confirmed that both hematopoietic and nonhematopoietic cells contribute to impaired early clonal deletion in mCat Tg mice, suggesting roles for redox regulation of autophagy in both cTECs and cortical DCs. It is not clear what cell-intrinsic effects overexpression of catalase may have in lymphocytes themselves, since they naturally express very high levels of catalase (4), and we did not detect any differences in $H_2O_2$ levels or autophagy in lymphocytes in mCat Tg mice, but our studies do not exclude this possibility. We propose that the increased presence of autoimmune indicators in mCat Tg mice results from inefficient early clonal deletion due to diminished autophagy-dependent presentation of self-peptides by cortical DCs and inefficient late clonal deletion driven, in part, by diminished autophagy-dependent presentation of self-peptides by mTECs. However, further studies will be required to characterize the cellular and molecular mechanisms regulating these processes and to determine whether peripheral expression of the mCat Tg and $Becn1^{KI/KI}$ alleles contribute to differences in peripheral tolerance induction in these models. Taken together, our results suggest a metabolic mechanism by which the redox status of TSCs established by low catalase expression regulates central T cell tolerance in the thymus by promoting high levels of constitutive autophagy required for self-antigen presentation and T cell selection.

## Materials and Methods

**Mice.** Young (5- to 7-wk-old) C57BL/6J (JAX: 000664), mCat Tg ( Jax: 016197) (26) and CAG-RFP-EGFP-LC3 Tg mice (JAX: 027139) were purchased from The Jackson Laboratory at 4 to 6 wk of age. Breeding pairs for GFP-LC3 (23) and $Becn1^{KI/KI}$ (29) were generously provided by Dr. Beth Levine (University of Texas Southwestern Medical Center) before her passing. GFP-LC3 $Becn1^{KI/KI}$ mice were crossed with mCat Tg animals. All mice used in experiments were bred and maintained at The University of Texas Health San Antonio animal facility under specific pathogen-free conditions. Animal studies and all procedures were approved by the Institutional Animal Care and Use Committee.

**Stromal Cell Isolation.** For stromal isolation, thymi were harvested and chopped with scissors carefully. Fragments from these thymi were then passed several times through a pipet tip. The large thymus pieces were then allowed to settle, following which most of the supernatant that contained lymphoid cells was removed. The remaining fragments were digested with 0.125% collagenase for 10 min at 37 °C. This process of pipetting, sedimentation, and lymphoid cell removal was repeated three additional times, followed by a final digestion in 0.05% trypsin. After the final digestion, cells were washed, pelleted down by the process of centrifugation, resuspended, and were then stained with a mixture of fluorescent antibodies recognizing allophycocyanin (APC)-conjugated anti-CD45.2 (Ly-5, clone 104; eBioscience), APC-conjugated anti-CD11c (HL3; BD Pharmingen), PECy7-conjugated anti-EpCAM (G8.8), and biotinylated anti-Ly-51(6C3; Biolegend). Dead and/or dying cells were excluded by DAPI staining.

**DC Isolation.** For DC isolation, thymi were enzymatically digested as described above. After the final digestion, all the collected lymphoid cells, as well as stromal cells, were combined in one tube, washed, pelleted by centrifugation, and were then stained with PerCPCy5.5 conjugated with anti-CD45.2 (30-F11) antibody purchased from eBioscience and APC-conjugated anti-CD11c (HL3) purchased from BD Pharmingen. Dead and/or dying cells were excluded by staining with DAPI. For plasmacytoid DC and cDC analysis, cells were stained with CD45.2 and CD11c as described for lymphoid and stromal cells, and with biotin-conjugated anti-B220 (CD45R; RA3-6B2, Invitrogen), PE-Streptavidin (Biolegend), and PE-Cy7–conjugated anti-Sirpα (CD172; P84, Biolegend).

**Measurement of Mitochondrial $H_2O_2$.** Enzymatically digested lympho-stromal preparations (as described above) from WT and mCat Tg mice were treated with 150 mM $H_2O_2$ for 30 min at 37 °C in the dark. After washing, cells were stained for 20 min at 37 °C using the fluorescent probe MitoPY1 (Tocris Biosciences, no. 4428) at a final concentration of 10 mM in the dark and then were stained with antibodies recognizing CD45.2, EpCAM, and Ly51, as described above. Lymphoid cells ($CD45.2^+$), DCs ($CD45.2^+$ $CD11c^+$), mTECs ($EpCAM^+$, $Ly51^-$), and cTECs ($EpCAM^+$, $Ly51^+$) in the same sample were recognized by electronic gating after acquisition. Dead cells were excluded by DAPI staining.

**Splenocyte Isolation.** Spleens obtained from mice were mashed in a Petri dish containing 3 mL of complete Roswell Park Memorial Institute (RPMI) medium (1×) (HyClone RPMI-1640, catalog no. SH30096.01; glutamine, streptomycin, penicillin, and nonessential amino acids were added) with 10% fetal bovine serum (FBS). The cell suspension was transferred to a fluorescence-activated cell sorting (FACS) tube, and centrifuged at 1,500 rpm for 5 min at 4 °C. The pellet was resuspended in 1 mL of 1× ammonium–chloride–potassium buffer to lyse red blood cells and pelleted again. The pellet was resuspended in 2 mL of RPMI buffer. Cells were counted using Trypan blue prior to staining and stimulation experiments.

**In Vitro Stimulation of Splenic T Cells.** Splenocytes from young WT and GFP-LC3 reporter mice were isolated and counted using a hemocytometer. Subsequently, $2 \times 10^6$ splenocytes were cultured for 24 h or 48 h with either anti-CD3 (145-2C11) and anti-CD28 (for stimulation group or with IL-7 for nonstimulation group) in flat-bottom 96-well plates. After 24 h, the stimulated cells were stained with PE-Cy7 conjugated anti-CD69 (H1.2F3) purchased from Biolegend and PerCP-efluor 710 conjugated anti-CD90.2 (30H12) purchased from eBioscience. Cells were analyzed using a BD LSRII flow cytometer and data were analyzed using FlowJo software (Tree Star).

**Immunofluorescence Microscopy from Cytospin.** For microscopic quantification of autophagic punctae after stimulation, 1 million cells were fixed with ice-cold acetone on to poly-L-lysine-coated slides (Sigma Aldrich) using a cytospin. Cells were then fixed with 4% paraformaldehyde for 20 min, then washed with phosphate-buffered saline with Tween (PBST; 3×), followed by permeabilization with 0.5% triton for 20 min, then washed with PBST (3×). After permeabilization, cells were blocked with 5% FBS in PBS for 30 min at room temperature. Cells were then incubated overnight at 4 °C with Alexa-Fluor-594 conjugated with anti-GFP in 0.1% (vol/vol) in PBS. The next day, cells were washed with PBST (3×), stained with DAPI for 30 min, washed with PBST (3×), and mounted with ProLong Gold antifade reagent. Images were captured on a Zeiss LSM710 confocal microscope.

**Autophagy Analysis by Flow Cytometry.** Lympho-stromal preparations (described above) from GFP-LC3 reporter mice with or without the mCat Tg and with or without $Becn1^{KI}$ alleles, and RFP-GFP-LC3 reporter mice with or without the mCat Tg were stained with antibodies recognizing CD45.2, CD11c, EpCAM, and Ly51, as described above. Autophagy was measured as GFP MFI. For lymphocyte, mTEC, and cTEC experiments, GFP MFI was normalized to GFP MFI in GFP-LC3–WT nonreporter control samples of the same cell type analyzed in the same experiment. For DCs, MFI was normalized to GFP-LC3 reporter plus mCat non-Tg (control) TECs analyzed in the same experiment. Dead cells were excluded by DAPI staining.

**Autophagy Analysis by Microscopy.** Thymi harvested from RFP-GFP-LC3 mCat non-Tg and mCat Tg mice were fixed in fresh 4% paraformaldehyde overnight, rocking at 4 °C. The next day, fixative was removed and replaced with 10% sucrose for 4 h, followed by 20% sucrose for 4 h, and 30% sucrose overnight. The next morning, tissues were placed vertically in embedding molds filled with optimal cutting temperature compound (Fisher no. 23–730-571) and frozen for 15 to 30 min on dry ice. Sections (10 μm thick) were cut and prepared for imaging by washing slides in PBS for 5 min, followed by two 5-min washes with 5% FBS in PBS and two 5-min washes with PBS. Coverslips were mounted with Vectashield Vibrance Antifade Mounting Medium with DAPI (Vector

Laboratories, no. H-1800). All imaging was performed on a Zeiss Axio Imager Z1 microscope using ZenPro software, version 2.3. Images in the GFP channel were captured at ×20 magnification using the Apotome attachment. Standardized exposure times were used to capture representative images from RFP-GFP-LC3 mCat non-Tg and mCat Tg tissues. Images were analyzed with ImageJ software (60, 61), similar to the approach previously described by Arias-Fuenzalida et al. (30). Briefly, a maximal Z projection was generated for each image (image > stacks > Z-project [projection type max intensity]), which was used for further analysis. A brightened image (image > adjust > brightness/contrast) was generated and the polygon-shape tool was used to outline and measure the thymic cortex using the region of interest (ROI) manager. Two copies of the original Z projection image were then made. A Gaussian blur filter (process > filters > Gaussian blur) was then applied to each copy with sigma set to 2 (copy 1) or 1 (copy 2), followed by subtraction of the filtered images (process > image calculator > copy 2, subtract, copy 1). A representative image is labeled "Difference of Gaussian Blurs" in Fig. 4. This image was used to generate a threshold image (image > adjust > threshold [Moment, B&W, dark background, auto]). Punctae were counted in the thresholded image using analyze > analyze particles > (size 0 to 5 μm, show: count masks). A representative image of the particles identified is labeled "ROI mask (5 mm threshold)" in Fig. 4. The number of punctae/$\mu m^2$ was compared by Student's *t* test in Prism, as described below.

**T Cell Clonal Deletion Assay.** Cleaved caspase 3 staining was performed using C57BL6 mice (5 wk and 6 mo) and mCat Tg mice (6 mo old), as we reported previously (62) and as described by Breed et al. (34). Single-cell suspensions were then stained for 30 min at 4 °C with the following antibodies: PE-Cy7–conjugated anti-CCR7 (4B12), APC-conjugated anti-CD19 (6D5), CD25 (PC61), NK1.1 (PK136), TCRγ/∂ (GL3), and PerCPCy5.5-conjugated TCRβ (H57-597), purchased from BioLegend. Fluorescein isothiocyanate-conjugated anti-CD5 (53-7.3) was purchased from Invitrogen. R-phycoerythrin–conjugated goat anti–rabbit IgG was purchased from Thermo Fisher. For staining with anti-cleaved caspase 3 (Asp175) (D3E9; Cell Signaling Technologies), cells were processed as immediately as possible after harvest to minimize cell death. Single-cell suspensions were generated in cold mouse tonicity Hank's balanced salt solutionHc (Hanks' balanced salt solution; GIBCO) with 5% FBS and 5 μg/mL DNase, by releasing the thymocytes from the harvested thymus by applying gentle mechanical force in circular motion to the thymus using the back of the Eppendorf tube. After the surface staining, cells were fixed with Cytofix/Cytoperm (BD Biosciences) for 30 min at 4 °C. Subsequent cells were washed with Perm/Wash buffer (BD Biosciences) and then stained with anti-cleaved caspase 3 at a 1:200 dilution for 30 min at 23 °C in the dark followed by staining with R-phycoerythrin goat anti–rabbit IgG for 30 min at 23 °C in the dark. Samples were analyzed using an LSR II flow cytometer (BD Biosciences) and FlowJo software (Tree Star).

**Positive Selection Analysis.** Single-cell suspensions were stained with FITC-conjugated anti-CD3 (145-2c11, Biolegend), APC-Cy7–conjugated anti-CD4 RM4-4 (Biolegend), V500-conjugated anti-CD8 (53-6,7; BD Bioscience), and PE-Cy7–conjugated anti-CD69 (H1.2F3, Biolegend).

**Treg Analysis.** Single-cell suspensions were stained with PE-conjugated anti-CD4 (GK1.5, eBioscience), V500-conjugated anti-CD8 (53-6,7; BD Bioscience), fixed and permeabilized as described above, and stained with PE-Cy7–conjugated anti-FoxP3 (FJK-16s, eBioscience) overnight at 4 °C. After washing, samples were analyzed using an LSR II flow cytometer (BD Biosciences) and FlowJo software (Tree Star).

**Chemokine Expression qRT-PCR.** TSCs were enriched with collagenase as described above, and single-cell suspensions were stained with APC-conjugated anti-CD45.2 (clone 104, Invitrogen), PE-Cy7–conjugated anti-EpCAM (CD236, G8.8 Biolegend), biotin-conjugated anti-Ly51 (6C3; Biolegend), and PE-conjugated streptavidin (Biolegend). CD45-EpCAM-Ly51$^-$ mTECs were subsequently sorted using a BD FACSAria cell sorter (BD Biosciences) using the single-cell sorting mode. qRT-PCR was performed as previously described (62). Briefly, RNA was isolated using the RNAqueous Micro Kit (Invitrogen) per manufacturer's instructions. cDNA synthesis was performed using a SuperScript VILO cDNA synthesis kit (Invitrogen) per manufacturer's instructions. cDNA preamplification was performed using the TaqMan PreAmp Master Mix Kit (catalog no. 4384267, ThermoFisher Scientific) per manufacturer's instructions. qPCR (cycle 1: 95 °C for 10 min; cycle 2, ×40: 95 °C for 15 s and 60 °C for 1 min) was performed using a BioRad CFX96 Real-Time System and C1000 Touch Thermal Cycler using presynthesized TaqMan Gene Expression Assay Probes (ThermoFisher Scientific) to amplify the following genes: *Ccl19* (Assay identification [ID]: Mm03646971_gH), *Ccl21a* (Assay ID: Mm00839966_g1), and *Hprt* (Assay ID: Mm00446968_m1). Gene expression values were analyzed using Bio-Rad CFX Manager software and normalized to Hprt.

**Reciprocal BMT.** Donor BM was obtained from young, hemizygous mCat Tg mice or WT littermate controls. T cell–depleted BM was prepared by cell sorting CD3$^-$ cells (using APC-conjugated anti-CD3; 145-2C11, Biolegend). T cell–depleted BM cells were transplanted by retro-orbital injection into mCat Tg or WT mice that were irradiated 24 h prior with 1,000 rad, using a cesium source gamma irradiator. Thymic cellularity and T cell clonal deletion were evaluated 6 wk later.

**Histology.** To assess immunopathology in mice, lungs and livers of 6- to 8-mo-old WT, mCat Tg, and mCat Tg Becn1$^{KI/KI}$ mice were paraffin-fixed and stained with H&E. Sections from at least three different anatomic areas were examined for lymphocytic infiltration in each tissue. Samples were coded and evaluated for the presence of lymphocytic infiltrates blinded.

**Antinuclear Antibody.** ANAs were evaluated by blind review in serum (1:100 dilution) of 6- to 8-mo-old WT, mCat Tg, and mCat Tg Becn1$^{KI/KI}$ mice using FITC-conjugated anti-IgG (poly4060) purchased from Biolegend on Hep-2 slides (MBL International). Images were captured using a Zeiss LSM710 microscope. Samples were coded and evaluation was performed blinded.

**Statistics.** Groups were compared as previously described (62). *P* values were calculated in GraphPad Prism 8 software using two-tailed unpaired Student's *t* test or ordinary one-way ANOVA. $P < 0.05$ indicated data were statistically significant, and significance is indicated in figure legends.

**Data Availability.** All study data are included in the article and/or supporting information.

**ACKNOWLEDGMENTS.** The Becn1 KI mice were kindly provided by Dr. Beth Levine before her passing. We greatly appreciate her generosity in sharing the mice as well as her time and expertise. The GFP-LC3 mice were generously shared with permission from Dr. Noboru Mizushima. The authors thank Drs. Nu Zhang and Shruti Mishra for help with T cell stimulation and lymphocytic infiltrate evaluation, and Yijiang Xu and Dr. Paolo Casali's laboratory for the use of the cytospin. This work was supported by NIH Public Health Service grant R01AI121367, by the Conklyn Family Endowment in Autoimmune Research, by NIH National Institute of General Medical Sciences grant R25GM130437 (to S.E.), and by funds from the UT Health San Antonio to A.V.G.

Author affiliations: [a]Department of Microbiology, Immunology and Molecular Genetics, University of Texas Long School of Medicine, UT Health San Antonio, San Antonio, TX 78229; [b]Barshop Institute for Longevity and Aging Studies, UT Health San Antonio, San Antonio, TX 78229; [c]Department of Medicine, Blood and Marrow Transplantation Division, Stanford University, Stanford, CA 94305; and [d]Department of Immunology, University of Texas Southwestern Medical Center, Dallas, TX 75390

1. D. H. Gray *et al.*, Unbiased analysis, enrichment and purification of thymic stromal cells. *J. Immunol. Methods* **329**, 56–66 (2008).
2. M. Mohtashami, J. C. Zúñiga-Pflücker, Three-dimensional architecture of the thymus is required to maintain delta-like expression necessary for inducing T cell development. *J. Immunol.* **176**, 730–734 (2006).
3. A. V. Griffith *et al.*, Spatial mapping of thymic stromal microenvironments reveals unique features influencing T lymphoid differentiation. *Immunity* **31**, 999–1009 (2009).
4. A. V. Griffith *et al.*, Metabolic damage and premature thymus aging caused by stromal catalase deficiency. *Cell Rep.* **12**, 1071–1079 (2015).
5. S. Cepeda, A. V. Griffith, Thymic stromal cells: Roles in atrophy and age-associated dysfunction of the thymus. *Exp. Gerontol.* **105**, 113–117 (2018).
6. M. K. Semwal, N. E. Jones, A. V. Griffith, Metabolic regulation of thymic epithelial cell function. *Front. Immunol.* **12**, 636072 (2021).

7. E. F. Lind, S. E. Prockop, H. E. Porritt, H. T. Petrie, Mapping precursor movement through the postnatal thymus reveals specific microenvironments supporting defined stages of early lymphoid development. *J. Exp. Med.* **194**, 127–134 (2001).
8. C. Penit, Localization and phenotype of cycling and post-cycling murine thymocytes studied by simultaneous detection of bromodeoxyuridine and surface antigens. *J. Histochem. Cytochem.* **36**, 473–478 (1988).
9. H. T. Petrie, J. C. Zúñiga-Pflücker, Zoned out: Functional mapping of stromal signaling microenvironments in the thymus. *Annu. Rev. Immunol.* **25**, 649–679 (2007).
10. L. Diebold, N. S. Chandel, Mitochondrial ROS regulation of proliferating cells. *Free Radic. Biol. Med.* **100**, 86–93 (2016).
11. E. Taniguchi Ishikawa *et al.*, Connexin-43 prevents hematopoietic stem cell senescence through transfer of reactive oxygen species to bone marrow stromal cells. *Proc. Natl. Acad. Sci. U.S.A.* **109**, 9071–9076 (2012).
12. J. Liu *et al.*, Bmi1 regulates mitochondrial function and the DNA damage response pathway. *Nature* **459**, 387–392 (2009).
13. K. M. Holmström, T. Finkel, Cellular mechanisms and physiological consequences of redox-dependent signalling. *Nat. Rev. Mol. Cell Biol.* **15**, 411–421 (2014).
14. K. T. Turpaev, Reactive oxygen species and regulation of gene expression. *Biochemistry (Mosc.)* **67**, 281–292 (2002).
15. G. Filomeni, E. Desideri, S. Cardaci, G. Rotilio, M. R. Ciriolo, Under the ROS … thiol network is the principal suspect for autophagy commitment. *Autophagy* **6**, 999–1005 (2010).
16. G. Filomeni, D. De Zio, F. Cecconi, Oxidative stress and autophagy: The clash between damage and metabolic needs. *Cell Death Differ.* **22**, 377–388 (2015).
17. R. Scherz-Shouval *et al.*, Reactive oxygen species are essential for autophagy and specifically regulate the activity of Atg4. *EMBO J.* **26**, 1749–1760 (2007).
18. R. Scherz-Shouval, Z. Elazar, ROS, mitochondria and the regulation of autophagy. *Trends Cell Biol.* **17**, 422–427 (2007).
19. E. E. Essick, F. Sam, Oxidative stress and autophagy in cardiac disease, neurological disorders, aging and cancer. *Oxid. Med. Cell. Longev.* **3**, 168–177 (2010).
20. H. Mancilla *et al.*, Glutathione depletion induces spermatogonial cell autophagy. *J. Cell. Biochem.* **116**, 2283–2292 (2015).
21. S. Zhao *et al.*, H2O2 treatment or serum deprivation induces autophagy and apoptosis in naked mole-rat skin fibroblasts by inhibiting the PI3K/Akt signaling pathway. *Oncotarget* **7**, 84839–84850 (2016).
22. Y. Chen, E. McMillan-Ward, J. Kong, S. J. Israels, S. B. Gibson, Oxidative stress induces autophagic cell death independent of apoptosis in transformed and cancer cells. *Cell Death Differ.* **15**, 171–182 (2008).
23. N. Mizushima, A. Yamamoto, M. Matsui, T. Yoshimori, Y. Ohsumi, In vivo analysis of autophagy in response to nutrient starvation using transgenic mice expressing a fluorescent autophagosome marker. *Mol. Biol. Cell* **15**, 1101–1111 (2004).
24. J. Nedjic, M. Aichinger, J. Emmerich, N. Mizushima, L. Klein, Autophagy in thymic epithelium shapes the T-cell repertoire and is essential for tolerance. *Nature* **455**, 396–400 (2008).
25. M. Aichinger, C. Wu, J. Nedjic, L. Klein, Macroautophagy substrates are loaded onto MHC class II of medullary thymic epithelial cells for central tolerance. *J. Exp. Med.* **210**, 287–300 (2013).
26. S. E. Schriner *et al.*, Extension of murine life span by overexpression of catalase targeted to mitochondria. *Science* **308**, 1909–1911 (2005).
27. D. J. Klionsky *et al.*, Guidelines for the use and interpretation of assays for monitoring autophagy. *Autophagy* **8**, 445–544 (2012).
28. H. H. Pua, I. Dzhagalov, M. Chuck, N. Mizushima, Y.-W. He, A critical role for the autophagy gene Atg5 in T cell survival and proliferation. *J. Exp. Med.* **204**, 25–31 (2007).
29. A. F. Fernández *et al.*, Disruption of the beclin 1-BCL2 autophagy regulatory complex promotes longevity in mice. *Nature* **558**, 136–140 (2018).
30. J. Arias-Fuenzalida *et al.*, Automated high-throughput high-content autophagy and mitophagy analysis platform. *Sci. Rep.* **9**, 9455 (2019).
31. L. Li, Z. V. Wang, J. A. Hill, F. Lin, New autophagy reporter mice reveal dynamics of proximal tubular autophagy. *J. Am. Soc. Nephrol.* **25**, 305–315 (2014).
32. G. Fu *et al.*, Themis controls thymocyte selection through regulation of T cell antigen receptor-mediated signaling. *Nat. Immunol.* **10**, 848–856 (2009).
33. S. Kim *et al.*, Regulation of positive and negative selection and TCR signaling during thymic T cell development by capicua. *eLife* **10**, e71769 (2021).
34. E. R. Breed, M. Watanabe, K. A. Hogquist, Measuring thymic clonal deletion at the population level. *J. Immunol.* **202**, 3226–3233 (2019).
35. D. Y. Hu *et al.*, A timeline demarcating two waves of clonal deletion and Foxp3 upregulation during thymocyte development. *Immunol. Cell Biol.* **94**, 357–366 (2016).
36. Z. Hu, J. N. Lancaster, L. I. Ehrlich, The contribution of chemokines and migration to the induction of central tolerance in the thymus. *Front. Immunol.* **6**, 398 (2015).
37. H. Kurobe *et al.*, CCR7-dependent cortex-to-medulla migration of positively selected thymocytes is essential for establishing central tolerance. *Immunity* **24**, 165–177 (2006).
38. T. Nitta, S. Nitta, Y. Lei, M. Lipp, Y. Takahama, CCR7-mediated migration of developing thymocytes to the medulla is essential for negative selection to tissue-restricted antigens. *Proc. Natl. Acad. Sci. U.S.A.* **106**, 17129–17133 (2009).
39. T. Ueno *et al.*, CCR7 signals are essential for cortex-medulla migration of developing thymocytes. *J. Exp. Med.* **200**, 493–505 (2004).
40. C. Paludan *et al.*, Endogenous MHC class II processing of a viral nuclear antigen after autophagy. *Science* **307**, 593–596 (2005).
41. H. M. Lee, J. L. Bautista, J. Scott-Browne, J. F. Mohan, C. S. Hsieh, A broad range of self-reactivity drives thymic regulatory T cell selection to limit responses to self. *Immunity* **37**, 475–486 (2012).
42. L. Klein, B. Kyewski, P. M. Allen, K. A. Hogquist, Positive and negative selection of the T cell repertoire: What thymocytes see (and don't see). *Nat. Rev. Immunol.* **14**, 377–391 (2014).
43. R. Bonasio *et al.*, Clonal deletion of thymocytes by circulating dendritic cells homing to the thymus. *Nat. Immunol.* **7**, 1092–1100 (2006).
44. C. Koble, B. Kyewski, The thymic medulla: A unique microenvironment for intercellular self-antigen transfer. *J. Exp. Med.* **206**, 1505–1513 (2009).
45. C. J. Kroger, N. A. Spidale, B. Wang, R. Tisch, Thymic dendritic cell subsets display distinct efficiencies and mechanisms of intercellular MHC transfer. *J. Immunol.* **198**, 249–256 (2017).
46. J. N. Lancaster *et al.*, Live-cell imaging reveals the relative contributions of antigen-presenting cell subsets to thymic central tolerance. *Nat. Commun.* **10**, 2220 (2019).
47. J. S. A. Perry *et al.*, Distinct contributions of Aire and antigen-presenting-cell subsets to the generation of self-tolerance in the thymus. *Immunity* **41**, 414–426 (2014).
48. M. Vobořil *et al.*, A model of preferential pairing between epithelial and dendritic cells in thymic antigen transfer. *eLife* **11**, e71578 (2022).
49. J. Li, J. Park, D. Foss, I. Goldschneider, Thymus-homing peripheral dendritic cells constitute two of the three major subsets of dendritic cells in the steady-state thymus. *J. Exp. Med.* **206**, 607–622 (2009).
50. V. Michaels Lopez *et al.*, Intrathymic SIRPa cDC subsets organization in normal and stress conditions reveal another level of cDCs heterogeneity. *J. Leukoc. Biol.* 10.1002/JLB.1A0921-502RR. (2022).
51. M. Vobořil *et al.*, Toll-like receptor signaling in thymic epithelium controls monocyte-derived dendritic cell recruitment and Treg generation. *Nat. Commun.* **11**, 2361 (2020).
52. T. Okada *et al.*, Murine thymic plasmacytoid dendritic cells. *Eur. J. Immunol.* **33**, 1012–1019 (2003).
53. M. H. Lahoud *et al.*, Signal regulatory protein molecules are differentially expressed by CD8- dendritic cells. *J. Immunol.* **177**, 372–382 (2006).
54. T. Ueno *et al.*, Role for CCR7 ligands in the emigration of newly generated T lymphocytes from the neonatal thymus. *Immunity* **16**, 205–218 (2002).
55. M. Kozai *et al.*, Essential role of CCL21 in establishment of central self-tolerance in T cells. *J. Exp. Med.* **214**, 1925–1935 (2017).
56. L. I. Ehrlich, D. Y. Oh, I. L. Weissman, R. S. Lewis, Differential contribution of chemotaxis and substrate restriction to segregation of immature and mature thymocytes. *Immunity* **31**, 986–998 (2009).
57. T. M. McCaughtry, T. A. Baldwin, M. S. Wilken, K. A. Hogquist, Clonal deletion of thymocytes can occur in the cortex with no involvement of the medulla. *J. Exp. Med.* **205**, 2575–2584 (2008).
58. D. Schmid, M. Pypaert, C. Münz, Antigen-loading compartments for major histocompatibility complex class II molecules continuously receive input from autophagosomes. *Immunity* **26**, 79–92 (2007).
59. C. Münz, Antigen processing via autophagy–Not only for MHC class II presentation anymore? *Curr. Opin. Immunol.* **22**, 89–93 (2010).
60. C. A. Schneider, W. S. Rasband, K. W. Eliceiri, NIH Image to ImageJ: 25 years of image analysis. *Nat. Methods* **9**, 671–675 (2012).
61. J. Schindelin *et al.*, Fiji: An open-source platform for biological-image analysis. *Nat. Methods* **9**, 676–682 (2012).
62. A. K. Hester *et al.*, Redox regulation of age-associated defects in generation and maintenance of T cell self-tolerance and immunity to foreign antigens. *Cell Rep.* **38**, 110363 (2022).